Identifying generalised segmental acceleration patterns that contribute to ground reaction force features across different running tasks

Original research article

Authors:

Jasper Verheul[1], John Warmenhoven[2,3], Paulo Lisboa[4], Warren Gregson[1], Jos Vanrenterghem[5], Mark A. Robinson[1]

1. Research Institute for Sport and Exercise Sciences, Liverpool John Moores University, Liverpool, United Kingdom
2. Department of Exercise and Sports Science, The University of Sydney, Lidcombe, Australia
3. Performance People & Teams, Australian Institute of Sport, Canberra, Australia
4. Department of Applied Mathematics, Liverpool John Moores University, Liverpool, United Kingdom
5. Department of Rehabilitation Sciences, KU Leuven, Leuven, Belgium

Corresponding Author:

Jasper Verheul (J.P.Verheul@ljmu.ac.uk)

Research Institute for Sport and Exercise Sciences, Liverpool John Moores University

Tom Reilly Building, Byrom Street, L3 5AF, Liverpool, United Kingdom

Abstract word count: 232

Text-only word count: 3041

Number of figures and tables: 2 figures and 1 table

Abstract

Objective: To support future developments of field-based biomechanical load monitoring tools, this study aimed to identify generalised segmental acceleration patterns and their contribution to ground reaction forces (GRFs) across different running tasks.

Design: Exploratory experimental design.

Methods: A multivariate principal component analysis (PCA) was applied to a combination of segmental acceleration data from all body segments for fifteen team-sport athletes performing accelerated, decelerated and constant low-, moderate- and high-speed running, and 90° cutting trials. Segmental acceleration profiles were then reconstructed from each principal component (PC) and used to calculate their specific GRF contributions.

Results: The first PC explained 48.57% of the acceleration variability for all body segments and was primarily related to the between-task differences in the overall magnitude of the GRF impulse. Magnitude and timing of high-frequency acceleration and GRF features (i.e. impact related characteristics) were primarily explained by the second PC (12.43%) and also revealed important between-task differences. The most important GRF characteristics were explained by the first five PCs, while PCs beyond that primarily contained small contributions to the overall GRF impulse.

Conclusions: These findings show that a multivariate PCA approach can reveal generalised acceleration patterns and specific segmental contributions to GRF features, but their relative importance for different running activities are task dependent. Using segmental acceleration to assess whole-body biomechanical loading generically across various movements may thus require task identification algorithms and/or advanced sensor or data fusion approaches.

Keywords: Biomechanical loading; Principal component analysis; Segmental contributions; Running; Accelerations

Practical Implications

- A multivariate PCA approach can be used to simultaneously identify general segmental coordination patterns and specific segment contributions to GRF across running tasks, but segment contributions to GRF vary between different movements.
- Caution should be practiced when using segmental acceleration signals to evaluate biomechanical loads (e.g. from popular body-worn accelerometers), especially across different tasks.
- Segmental acceleration information likely requires task identification algorithms and/or advanced sensor or data fusion approaches to assess whole-body biomechanical loading generically across various running movements.

Introduction

Although the physiological demands of sports have been monitored and investigated extensively in the field, biomechanical loads are still poorly quantified and not well understood [1]. Ground reaction forces (GRF) have, therefore, been suggested as a measure of external whole-body biomechanical loading, which might be estimated from currently popular body-worn accelerometers [2,3]. Estimating GRF from single accelerometers is, however, not straightforward [4–6]. Whilst there might be the potential of using full-body segmental accelerations to estimate GRF, reducing the number of segments to a number more feasible in a practical setting has been shown to substantially increase the GRF error [2,7]. These findings collectively suggest that estimating whole GRF waveforms accurately from segmental accelerations across different tasks is unlikely to be feasible. Since human running comprises a complex combination of simultaneous segmental movements however, more complex analyses may identify fundamental movement features that contribute to the GRF and could still be captured with accelerometers.

Principal component analysis (PCA) is a technique that can be used to reduce the amount of redundant information and extract key characteristics (e.g. magnitude, difference and phase shift operators [13,20]) of highly-dimensional biomechanical data. For example, PCA has been used to analyse gait patterns [8–10] and postural control [11,12], differentiate between pathological groups [10,13,14], or quantify and evaluate sports technique [15–17]. Although applications of PCA in biomechanics have typically focussed on waveform data for individual variables, multivariate PCA approaches allow for structures of variability to be uncovered across multiple parameters at the same time [8,9,15]. Given the complexity of segment coordination and interdependency of segmental accelerations during human running, a simultaneous analysis of multiple acceleration profiles is desirable to examine if generalised acceleration patterns across various segments exist and are related to specific GRF features. A multivariate PCA approach in which different variables (e.g. segments, tasks, time) are combined, might help to uncover such acceleration patterns and related GRF features across different running tasks, and reveal which specific segmental accelerations together influence changes in GRF profiles.

It is unlikely that GRF can be predicted from one or several segmental accelerations using mechanical methods [3,4,6]. However, these approaches typically use acceleration signals from predefined segments deemed important for GRF but do not allow for an agnostic identification of generalised multi-segmental contributions to the GRF. We hypothesised that if explicit GRF features are related to generalised acceleration patterns across different running tasks, this could further inform the potential for using segmental accelerations to assess whole-body biomechanical loads in running-based sports (such as the choice of relevant segments or the feasibility to generalise across tasks). Therefore, this study aimed to use a multivariate PCA approach to identify segmental acceleration patterns that contribute to GRF features, to more comprehensively understand biomechanical loading and support future developments of field-based biomechanical load monitoring tools.

Methods

Data. A previously described data set of full-body kinematics and GRF data for right foot contacts of fifteen healthy team-sport athletes (12 males and 3 females, age 23±4 years, height 178±9 cm, body mass 73±10 kg, sports participation 7±5 h per week) were used for this study [2]. This study was approved by the Liverpool John Moores University ethics committee and participants provided written informed consent according to the ethics regulations.

Participants performed accelerated, decelerated, low- (2-3 $m \cdot s^{-1}$) moderate- (4-5 $m \cdot s^{-1}$) and high-speed (>6 $m \cdot s^{-1}$ including maximal sprinting) running, and 90° cutting [2]. Seventy-six marker trajectories were measured from a three-dimensional motion capture system (Qualisys Inc., Gothenburg, Sweden), while GRFs were measured from a force platform (Kistler Holding AG, Winterthur, Switzerland). Kinematic and kinetic data were exported to Visual3D (C-motion, Germantown, MD, USA), which was used to build a fifteen segment (head, trunk, pelvis, upper arms, forearms, hands, thighs, shanks and feet) six-degree-of-freedom model [2]. Centre of mass (CoM) accelerations for each segment were calculated as the double differentiation of segmental CoM positions.

Normalisation and scaling. All fifteen segmental CoM acceleration and GRF waveforms in the mediolateral (x), anteroposterior (y) and vertical (z) direction during ground contact were normalised to 101 data points for each trial. Segmental accelerations were then expressed as

acceleration vectors **a** for every time point t (equation 1) (note: vectors and matrices will be referred to by using bold lowercase or capital letters respectively).

$$\mathbf{a}(t) = [ax_1(t), ay_1(t), az_1(t), ax_2(t), \dots, az_{15}(t)] \quad \text{Eq.1}$$

The combination of acceleration vectors for each trial thus formed a 101×45 acceleration matrix $\mathbf{A}^{\mathbf{trial}}$. Trial-specific acceleration matrices were then combined in participant- and task-specific matrices $\mathbf{A}^{\mathbf{part,task}}$ by vertically stacking each trial matrix $\mathbf{A}^{\mathbf{trial}}$ per participant and task. These combined acceleration matrices $\mathbf{A}^{\mathbf{part,task}}$ were normalised and scaled to 1) assure that every participant equally contributed to the variance of the total acceleration matrix, 2) reduce anthropometric differences between participants, 3) preserve relative segmental acceleration amplitudes and 4) correctly represent the portion of the total body mass of each segment [12]. First, a participant- and task-specific mean acceleration vector $\overline{\mathbf{a}^{\mathbf{part,task}}}$ was calculated and subtracted from each acceleration vector **a** (equation 2), to assure that the first PC described the direction of maximum variance in the segmental acceleration data.

$$\mathbf{A}^{\mathbf{part,task'}}(t) = \left[\left(ax_1(t) - \overline{ax_1{}^{part,task}}\right), \left(ay_1(t) - \overline{ay_1{}^{part,task}}\right), \dots, \left(az_{15}(t) - \overline{az_{15}{}^{part,task}}\right)\right] \quad \text{Eq.2}$$

Matrix $\mathbf{A}^{\mathbf{subj,task'}}$ thus represented the acceleration deviations from the participant's mean segmental acceleration for each task. Secondly, acceleration vectors for each participant were divided by the mean Euclidean norm $\overline{\mathbf{euc}_{\mathbf{norm}}{}^{\mathbf{part,task}}}$ of all acceleration vectors (equation 3), to ensure that participants equally contributed to the variance of the total acceleration matrix and to minimise amplitude differences due to anthropometric differences [11,18].

$$\mathbf{A}^{\mathbf{part,task''}}(t) = \frac{\mathbf{A}^{\mathbf{part,task'}}(t)}{\mathbf{euc}_{\mathbf{norm}}{}^{\mathbf{part,task}}} \quad \text{Eq.3}$$

Thirdly, each acceleration vector was normalised for the relative segmental masses to further account for anthropometric differences between segments. Acceleration vectors were multiplied by a weight vector **w** (equation 4), which contained mass ratios of each segment relative to the total body mass [19].

$$\mathbf{A}^{\mathbf{part,task'''}}(t) = \mathbf{w} \cdot \mathbf{A}^{\mathbf{part,task''}}(t) \quad \text{Eq.4}$$

Finally, the participant- and task-specific acceleration matrices for each participant $\mathbf{A}^{\mathbf{part,task'''}}$ were combined in one 48783×45 (15 participants · 6 tasks · number of trials per task (483 in total) · 101 data points per trial) acceleration matrix **A**.

Principal component analysis. A PCA was performed on the normalised and combined acceleration matrix **A**. The results included 1) eigenvector matrix **EV** consisting of 45 orthogonal eigenvectors $\mathbf{ev_k}$, (or 'principal component vectors') each indicating the largest acceleration variability for all segments, 2) eigenvalue matrix $\boldsymbol{\lambda}$ containing the eigenvalues $\boldsymbol{\lambda_k}$ which quantified the amount of variability described by each eigenvector $\mathbf{ev_k}$, with a strict decrease in the amount of variability with increasing k, and 3) time evolution coefficient matrix **C** (or 'score matrix') describing how the original segmental acceleration data evolved along the new principal acceleration axes. **C** was calculated by projecting each original normalised and scaled acceleration vector **a** onto each PC_k of the eigenvector matrix [12], according to equation 5.

$$\mathbf{c_k}(t) = \mathbf{a}(t) \cdot \mathbf{ev_k} \quad \text{Eq.5}$$

Principal accelerations and principal GRF. Participant- and task-specific principal acceleration (PA) matrices $\mathbf{PA}^{\mathbf{part,task}}$ were reconstructed for each individual PC_k (equation 6) to investigate how patterns of acceleration contribute to the GRF, or the sum of the first k PCs (equation 7) to examine the number of PCs required to adequately describe the whole GRF waveform. PCs were expressed in the original segmental acceleration space by decomposing reconstructed acceleration matrices into participant- and task-specific matrices, after which the normalisation and scaling steps were retraced.

$$\mathbf{PA_k}^{\mathbf{part,task}}(t) = \overline{\mathbf{a}^{\mathbf{part,task}}} + \overline{\mathbf{euc_{norm}}^{\mathbf{part,task}}} \cdot \mathbf{w}^{-1} \cdot [\mathbf{C_k} \cdot \mathbf{ev_k}]^{\mathbf{part,task}} \quad \text{Eq.6}$$

$$\mathbf{PA_{1-k}}^{\mathbf{part,task}}(t) = \overline{\mathbf{a}^{\mathbf{part,task}}} + \overline{\mathbf{euc_{norm}}^{\mathbf{part,task}}} \cdot \mathbf{w}^{-1} \cdot \left[\sum_{\mathbf{k=1}}^{\mathbf{1,2,\ldots,45}} \mathbf{C_k} \cdot \mathbf{ev_k}\right]^{\mathbf{part,task}} \quad \text{Eq.7}$$

Since the reconstructed PAs are consistent with the laws of Newtonian mechanics, the principal segmental acceleration vectors **pa** can be used to calculate principal GRF (PGRF) profiles. PGRF was

defined as the part of the overall GRF that is associated with the totality of all segment PAs combined. Resultant PGRF curves were calculated as the sum of the product of each segmental mass and principal CoM acceleration in the three directions, from each individual PC_k (equation 8), or from the sum of PAs reconstructed from the first k PCs (equation 9; Fig. 1).

$$\mathbf{PGRF_k} = \sqrt{\left(\sum_{n=1}^{15}(\mathbf{pa_{k,n,x}} \cdot m_n)\right)^2 + \left(\sum_{n=1}^{15}(\mathbf{pa_{k,n,y}} \cdot m_n)\right)^2 + \left(\sum_{n=1}^{15}(\mathbf{pa_{k,n,z}} \cdot m_n) + g \cdot BM\right)^2} \quad \text{Eq. 8}$$

$$\sum \mathbf{PGRF_{1-k}} = \sum_{pc=1}^{k}\left[\sqrt{\left(\sum_{n=1}^{15}(\mathbf{pa_{k,n,x}} \cdot m_n)\right)^2 + \left(\sum_{n=1}^{15}(\mathbf{pa_{k,n,y}} \cdot m_n)\right)^2 + \left(\sum_{n=1}^{15}(\mathbf{pa_{k,n,z}} \cdot m_n) + g \cdot BM\right)^2}\right] \quad \text{Eq. 9}$$

In which k is the PC number, **pa** the principal segmental acceleration in x, y or z direction, m the segmental mass, n the number of segments (n=15), g the gravitational acceleration (-9.81 $m \cdot s^{-1}$) and BM the total body mass. Measured and calculated PGRF curves were normalised to each participant's body mass and accuracy evaluated as the curve root mean squared error (RMSE) relative to the measured GRF.

Results

Visual screening of PC results revealed that distinct acceleration and GRF features were primarily explained by the first five PCs, which explained 77.8% of all segmental acceleration variability across participants and tasks. Each additional PC (i.e. k>5) explained <3% variance of the original acceleration data and contributed <1% to the overall GRF. Therefore, only the first five PGRF and ∑PGRF profiles (see Fig. 1 for an example), and associated PAs were used for further qualitative analysis.

PC_1 explained 48.6% of the acceleration variability of all segments, which accounted for the majority of the overall GRF impulse (Fig. 2; Table 1). The largest amplitude of PA_1 occurred between ~10-70% of stance (Fig. A.1 and A.2) for decelerated and constant-speed running, but later during stance (~30-90%) for accelerated running. PA_1 magnitudes were typically the lowest for 90° cutting and running at slower speeds and the highest for the forearms and hands.

Including PC_2 reduced ∑PGRF errors by 25.5% across tasks (Table 1). PC_2 primarily explained high-frequency acceleration contributions to the GRF impact peak associated with landing (Fig. 2), for all tasks except accelerations, and were primarily expressed in PA_2 profiles of the right thigh, shank and foot (stance leg segments) and pelvis. In contrast to the other tasks, $PGRF_2$ features for accelerated running occurred during the second half of stance (i.e. ~50-90%).

Segmental accelerations from PC_3 were associated with two GRF features for constant-speed running, but not for the other tasks. $PGRF_3$ contained small impact peak force components during early stance (~20-30%), as well as a general contribution to GRF impulse during the second half of stance (Fig. 2). Magnitudes for both GRF features increased with running speed and were primarily associated with accelerations of leg and arm segments (Fig. A.2).

Compared to the first three PCs, PC_4 and PC_5 contained considerably less segmental acceleration variability and distinct GRF features (Table 1). For accelerated running, these PCs made constant (but small) GRF contributions from ~10-80% ($PGRF_4$) and ~0-50% ($PGRF_5$) of stance (Fig. 2), while for other movements, PA_4 profiles were mainly associated with small GRF contributions during the first ~40% of stance. For high-speed running, $PGRF_5$ contained a considerable amount of GRF impulse, but not for the other tasks.

Including more PCs (i.e. k>5) gradually increased the overall GRF and reduced ∑PGRF errors but were not related to specific GRF features. To achieve ∑PGRF errors within 10% of the mean RMSE for GRF from all 45 PCs (i.e. the original data), a total of 18 (accelerations), 2 (decelerations), 15 (90° cuts), 7 (low-speed running), 4 (moderate-speed running) and 18 (high-speed running) PCs were required, respectively.

Discussion

Task-specific accelerations. The aim of this study was to identify key contributions of generalised acceleration patterns and specific segments to the GRF. The three primary modes of variation described by PCA; a magnitude operator, difference operator and phase shift [13,20], were evident in the first five PAs and PGRFs. First, segmental acceleration magnitude differences

associated with GRF impulse (i.e. overall loading of the body) and the impact peak were captured by PC_1 and PC_2 respectively. Substantial amplitude variability in PA and PGRF profiles between tasks showed that the magnitude of these GRF characteristics was strongly dependent on task (Fig. 2). Secondly, PC_3 and PC_5 highlighted difference operator features. For accelerated running for example, the main contributions of $PGRF_3$ and $PGRF_5$ to the overall GRF was during the first half of stance but explained a much lower amount of force during push-off, while for constant-speed running this was the other way around. Thirdly, clear phase shift characteristics were manifested in the first two PCs. For example, the impulse peak ($PGRF_1$) and high-frequency acceleration and force features of PC_2 appeared in the first ~10-40% of stance for decelerations, constant-speed running and cutting tasks, but much later during stance for accelerated running. These results show that PCA can identify general acceleration patterns underlying specific GRF profiles, as well as highlight the relative importance of these features for different running tasks.

PC_2 primarily contained acceleration and force features related to the GRF impact peak, for all tasks except accelerations. These force peaks were mostly explained by high PA_2 peaks of the support leg's foot, shank and thigh segment, and the pelvis to a lesser extent (Fig. A.1 and A.2). This supports previous suggestions that the impact peak is primarily associated with stance leg accelerations [21–23]. Moreover, despite the absence of visual impact peaks in GRF waveforms for non-rearfoot running gaits (e.g. sprinting), force frequencies associated with these initial force peaks are still present [24,25]. Clear impact force peaks were indeed found in $PGRF_2$ profiles for high-speed running, for which runners typically switched to a forefoot landing technique (Fig. 2). The present PCA approach thus further supports the presence of impact force peaks in non-rearfoot running, despite their visual absence in the GRF waveform.

For accelerated running, PA_2 profiles of the support leg's foot, shank and thigh segments were mainly related to a force peak during the second half of stance (Fig. 2). In addition, the smoother impacts of landing during accelerations were better explained by PC_5 and thus less important for the overall biomechanical load on the body. This highlights the importance of force production when pushing off the ground in acceleration movements, compared to other tasks in which braking (force) is emphasised

more. Using PCA across multiple tasks can thus not only identify generic acceleration patterns, but also explain their relative importance for different running movements.

The results of this study highlight that segment contributions to GRF are movement dependent. These findings could explain why generalised methods to predict GRF from one or a few acceleration signals cannot lead to accurate GRF estimates across different tasks [2,7]. For example, a specific segment (or combination of segments) might be suitable to estimate GRF profiles for sprinting, while the same segments are not so suitable to describe the GRF for decelerated running. Therefore, one should be cautious when using generic biomechanical models or approaches to estimate GRF and/or assess external biomechanical loads from segmental accelerations across different running tasks.

Segment-specific accelerations. Trunk accelerometry is arguably the most commonly used acceleration signal for assessing biomechanical loads in different sports [26–28]. Although the trunk is thought to be the main contributor to GRF [21], trunk PA_1 profiles were very similar to other segments, for all tasks (Fig. A.1 and A.2). Moreover, higher PCs (i.e. k>1) did not explain any considerable additional trunk acceleration features. These findings thus suggest that the trunk's large contributions to GRF are primarily due to its large mass rather than the characteristics of its acceleration. The value of using trunk accelerometry alone for biomechanical load monitoring purposes is thus probably limited.

PAs of the forearm and hand segments typically had a high magnitude of acceleration (Fig. A.1 and A.2) but did not make any distinct contribution to the specific GRF features in the first five PCs. Furthermore, for decelerated and low- to moderate-speed running considerably less PCs were required to achieve ∑PGRF errors within 10% of the mean RMSEs from all 45 PCs. This is possibly caused by the more profound and complex arm movements (explained by PCs beyond the first five) during acceleration, cutting and sprinting movements. Therefore, although arm movements (but also swing leg motion) are not the primary contributors to GRF, these segments do account for a considerable part of overall GRF impulse. These findings highlight that all segments should be considered when assessing whole-body loading, especially for sports in which dynamic and high-intensity tasks are frequently performed.

It should be acknowledged that directly measuring PAs (e.g. from multiple body-worn accelerometers) may not be feasible in training and competition environments, making it difficult to translate the present findings to a field-based load monitoring context. The multivariate PCA approach used in this study could, however, uncover a deeper layer of complexity and highlight key characteristics in a high-dimensional acceleration data set. This complexity adds to previous findings that reconstructing GRF waveforms from less than all segments across different tasks is unlikely feasible [2]. The PCA allowed for different acceleration combinations and key features to be detected, which provides practical insight for what sensors to include when using too many sensors is an issue in the field. Regardless, the complexity of segmental contributions to GRF outlined in this study further emphasises that estimating biomechanical loading from accelerations is not straightforward, especially across different tasks. Therefore, using body-worn accelerometry to estimate whole-body biomechanical loading across various movements likely requires task identification algorithms and/or advanced sensor or data fusion approaches (e.g.[29]).

Limitations. The methods described in this study have several limitations. First, PCA was deliberately performed on the combined segmental accelerations for multiple participants and tasks. The results are thus a general representation of how segmental acceleration contribute to GRF, across different running tasks. Unique loading or movement features for individual athletes or tasks may thus not be highlighted and future research could consider task- and/or participant-specific PCA. Secondly, using resultant accelerations and GRFs did not allow for identifying direction-specific acceleration and GRF features. However, this study aimed to evaluate generic acceleration patterns related to overall biomechanical load features. Moreover, body-worn accelerometers cannot typically distinguish between global x-y-z directions and using resultant accelerations was deemed more feasible for potential translations of our findings to a field-based load monitoring context. Thirdly, segmental acceleration data were normalised by a weighting vector based on a standardised mass distribution [19]. Due to typical anthropometric differences between participants, defining and applying an individualised mass distribution could affect the results. Although this was beyond the scope of this study, future work could consider if personalised normalisation may be beneficial.

Conclusions

This study aimed to identify general segmental acceleration patterns associated with GRF features that might be used to assess whole-body biomechanical loads. Although a multivariate PCA could reveal generic acceleration patterns and specific segmental contributions to GRF, the relative importance of these features varied between tasks. Using segmental acceleration to assess whole-body biomechanical loading generically across different movements thus likely requires task identification algorithms and/or advanced sensor or data fusion approaches.

Acknowledgements

This study did not receive any external financial support.

Supplementary files

Fig. A.1 and A.2 can be found in Appendix A, which is available as an online supplementary document.

References

1. Vanrenterghem J, Nedergaard NJ, Robinson MA, Drust B. Training Load Monitoring in Team Sports: A Novel Framework Separating Physiological and Biomechanical Load-Adaptation Pathways. *Sport Med*. 2017;47(11):2135-2142. doi:10.1007/s40279-017-0714-2

2. Verheul J, Gregson W, Lisboa PJ, Vanrenterghem J, Robinson MA. Whole-body biomechanical load in running-based sports: The validity of estimating ground reaction forces from segmental accelerations. *J Sci Med Sport*. 2019;22(6):716-722. doi:10.1016/j.jsams.2018.12.007

3. Nedergaard NJ, Robinson MA, Eusterwiemann E, Drust B, Lisboa PJ, Vanrenterghem J. The Relationship Between Whole-Body External Loading and Body-Worn Accelerometry During Team-Sport Movements. *Int J Sports Physiol Perform*. 2017;12(1):18-26. https://search.ebscohost.com/login.aspx?direct=true&db=sph&AN=121191349&site=ehost-live.

4. Nedergaard NJ, Verheul J, Drust B, et al. The feasibility of predicting ground reaction forces during running from a trunk accelerometry driven mass-spring-damper model. *PeerJ*. 2018;6:e6105. doi:10.7717/peerj.6105

5. Raper DP, Witchalls J, Philips EJ, Knight E, Drew MK, Waddington G. Use of a tibial accelerometer to measure ground reaction force in running: A reliability and validity comparison with force plates. *J Sci Med Sport*. 2018;21(1):84-88. doi:10.1016/j.jsams.2017.06.010

6. Edwards S, White S, Humphreys S, Robergs R, O'Dwyer N. Caution using data from triaxial accelerometers housed in player tracking units during running. *J Sports Sci*. 2018:1-9. doi:10.1080/02640414.2018.1527675

7. Pavei G, Seminati E, Cazzola D, Minetti AE. On the estimation accuracy of the 3D body center

of mass trajectory during human locomotion: Inverse vs. forward dynamics. *Front Physiol*. 2017;8(129):1-13. doi:10.3389/fphys.2017.00129

8. Daffertshofer A, Lamoth CJCC, Meijer OG, Beek PJ. PCA in studying coordination and variability: A tutorial. *Clin Biomech*. 2004;19(4):415-428. doi:10.1016/j.clinbiomech.2004.01.005

9. Troje NF. Decomposing biological motion: A framework for analysis and synthesis of human gait patterns. *J Vis*. 2002;2:371-387. http://journalofvision.org/2/5/2/.

10. Federolf PA, Boyer KA, Andriacchi TP. Application of principal component analysis in clinical gait research: Identification of systematic differences between healthy and medial knee-osteoarthritic gait. *J Biomech*. 2013;46(13):2173-2178. doi:10.1016/j.jbiomech.2013.06.032

11. Federolf PA, Roos L, Nigg BM. Analysis of the multi-segmental postural movement strategies utilized in bipedal, tandem and one-leg stance as quantified by a principal component decomposition of marker coordinates. *J Biomech*. 2013;46:2626-2633. doi:10.1016/j.jbiomech.2013.08.008

12. Federolf PA. A novel approach to study human posture control: “Principal movements” obtained from a principal component analysis of kinematic marker data. *J Biomech*. 2016;49:364-370. doi:10.1016/j.jbiomech.2015.12.030

13. Wrigley AT, Albert WJ, Deluzio KJ, Stevenson JM. Differentiating lifting technique between those who develop low back pain and those who do not. *Clin Biomech*. 2005;20:254-263. doi:10.1016/j.clinbiomech.2004.11.008

14. Deluzio KJ, Wyss UP, Zee B, Costigan PA, Sorbie C. Principal component models of knee kinematics and kinetics: Normal vs. pathological gait patterns. *Hum Mov Sci*. 1997;16:201-217. doi:10.1016/S0167-9457(96)00051-6

15. Federolf PA, Reid R, Gilgien M, Haugen P, Smith G. The application of principal component analysis to quantify technique in sports. *Scand J Med Sci Sports*. 2014;24:491-499. doi:10.1111/j.1600-0838.2012.01455.x

16. Boyer KA, Silvernail JF, Hamill J. The Role of Running Mileage on Coordination Patterns in Running. *J Appl Biomech*. 2014;30:649-654. doi:10.1123/JAB.2013-0261

17. Warmenhoven J, Cobley S, Draper C, Harrison A, Bargary N, Smith R. How gender and boat-side affect shape characteristics of force – angle profiles in single sculling: Insights from functional data analysis. *J Sci Med Sport*. 2018;21(5):533-537. doi:10.1016/j.jsams.2017.08.010

18. Gløersen Ø, Myklebust H, Hallén J, Federolf PA. Technique analysis in elite athletes using principal component analysis. *J Sports Sci*. 2018;36(2):229-237. doi:10.1080/02640414.2017.1298826

19. Dempster WT. Space requirements of the seated operator: Geometrical, Kinematic, and Mechanical Aspects of the Body With Special Reference to the Limbs. *WADC Tech Rep*. 1955:55-159.

20. Brandon SCE, Graham RB, Almosnino S, Sadler EM, Stevenson JM, Deluzio KJ. Interpreting principal components in biomechanics: Representative extremes and single component reconstruction. *J Electromyogr Kinesiol*. 2013;23:1304-1310. doi:10.1016/j.jelekin.2013.09.010

21. Bobbert MF, Schamhardt HC, Nigg BM. Calculation of vertical ground reaction force estimates during running from positional data. *J Biomech*. 1991;24(12):1095-1105. doi:10.1016/0021-9290(91)90002-5

22. Shorten M, Mientjes MIV. The “heel impact” force peak during running is neither “heel” nor “impact” and does not quantify shoe cushioning effects. *Footwear Sci*. 2011;3(1):41-58.

368 doi:10.1080/19424280.2010.542186

369 23. Clark KP, Ryan LJ, Weyand PG. A general relationship links gait mechanics and running
370 ground reaction forces. *J Exp Biol*. 2017;220(2):247-258. doi:10.1242/jeb.138057

371 24. Hamill J, Gruber AH. Is changing footstrike pattern beneficial to runners? *J Sport Heal Sci*.
372 2017;6:146-153. doi:10.1016/j.jshs.2017.02.004

373 25. Gruber AH, Edwards WB, Hamill J, Derrick TR, Boyer KA. A comparison of the ground
374 reaction force frequency content during rearfoot and non-rearfoot running patterns. *Gait*
375 *Posture*. 2017. doi:10.1016/j.gaitpost.2017.04.037

376 26. Colby MJ, Dawson B, Heasman J, Rogalski B, Gabbett TJ. Accelerometer and GPS-Derived
377 Running Loads and Injury Risk in Elite Australian Footballers. *J Strength Cond Res*.
378 2014;28(8):2244-2252.

379 27. Akenhead R, Marques JB, Paul DJ. Accelerometer load: a new way to measure fatigue during
380 repeated sprint training? *Sci Med Footb*. 2017;1(2):151-156.
381 doi:10.1080/24733938.2017.1330550

382 28. Buchheit M, Gray A, Morin J-B. Assessing stride variables and vertical stiffness with GPS-
383 embedded accelerometers: preliminary insights for the monitoring of neuromuscular fatigue on
384 the field. *J Sport Sci Med*. 2015;(14):698-701.

385 29. Johnson WR, Mian A, Robinson MA, Verheul J, Lloyd DG, Alderson JA. Multidimensional
386 ground reaction forces and moments from wearable sensor accelerations via deep learning.
387 *arXiv Prepr*. 2019.
388

Figures and tables

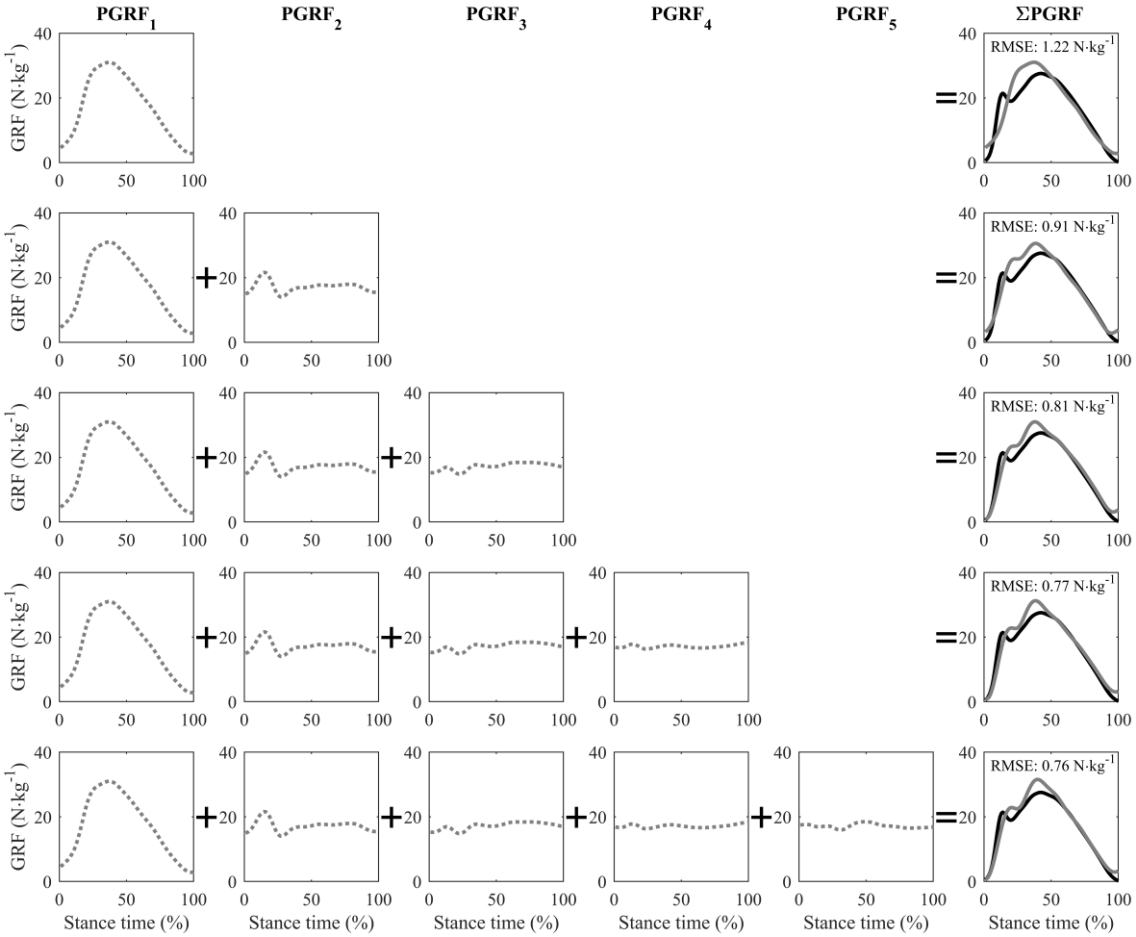

Figure 1 Representative example of individual and summed ground reaction force (GRF) profiles reconstructed from the first five principal components (PCs), for a single trial of running at a constant moderate speed. Individual principal GRFs (PGRFs; grey dotted lines) were added together as the summed PGRFs (∑PGRFs; grey solid lines) for the first k PCs and compared to the measured GRF (black solid line) by the curve root mean square error (RMSE).

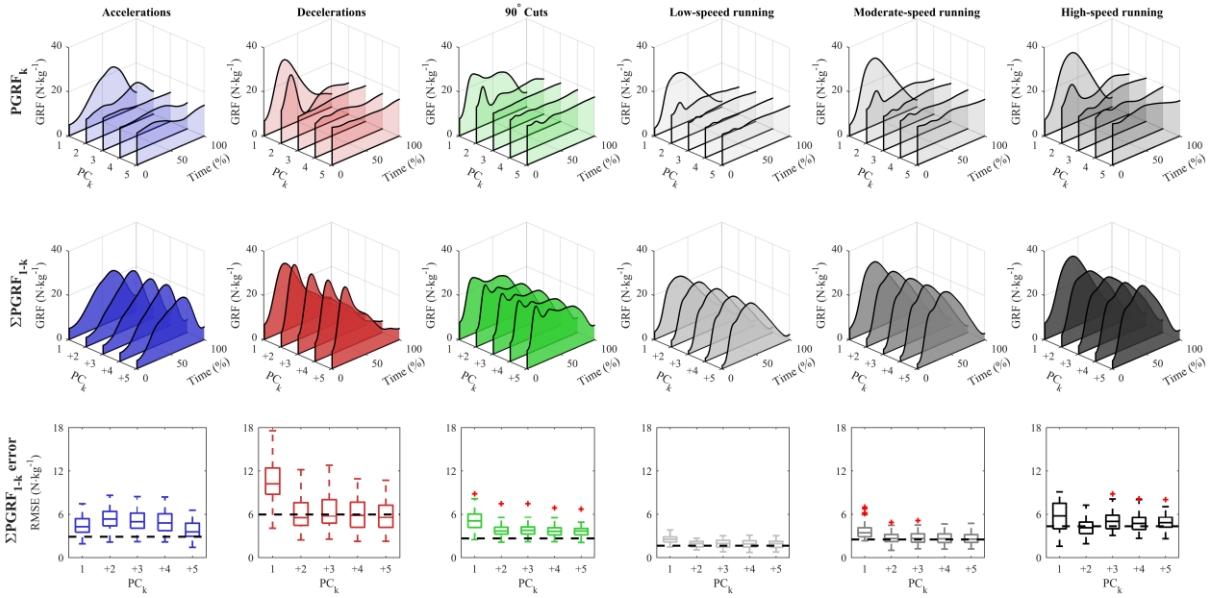

397

398 **Figure 2** Mean principal ground reaction forces (PGRFs) calculated from the first five principal
399 components (PCs), for each task. PGRFs were calculated from principal accelerations (PAs)
400 reconstructed from either the k^{th} PC (top row), or the sum of the first k PCs ($\sum PGRF_{1\text{-}k}$; middle row).
401 Root mean square errors (RMSE; middle row) are mean errors for the $\sum$PGRF profiles and the
402 horizontal black line represents the RMSE for $\sum$PGRFs from all 45 PCs (i.e. the original data).

Table 1 Principal components and ground reaction forces for the different tasks

	Principal components (k)					
	1	2	3	4	5	45
λ_k (%)	48.57	12.43	8.56	4.44	3.78	0
Cumulative λ (%)	48.57	60.99	69.55	73.99	77.77	100
	∑PGRF RMSE (N·kg^{-1})					
Accelerations (n=80)	4.46 ±1.3	5.37 ±1.5	5.09 ±1.5	4.93 ±1.5	3.88 ±1.2	2.89 ±0.7
Decelerations (n=83)	10.69 ±3.1	6.18 ±2.3	6.44 ±2.4	6.11 ±2.2	5.88 ±2	5.97 ±1.8
90° Cuts (n=88)	5.11 ±1.3	3.77 ±0.9	3.79 ±0.9	3.65 ±0.8	3.61 ±0.7	2.66 ±0.7
Constant speed running						
Low (2-3 m·s^{-1}; n=81)	2.53 ±0.5	1.89 ±0.4	1.93 ±0.5	1.92 ±0.5	1.87 ±0.5	1.65 ±0.4
Moderate (4-5 m·s^{-1}; n=80)	3.74 ±1.1	2.70 ±0.8	2.82 ±0.9	2.72 ±0.8	2.66 ±0.7	2.51 ±0.6
High (>6 m·s^{-1}; n=71)	5.67 ±2	4.14 ±1.2	5.03 ±1.2	4.71 ±1.2	4.84 ±1.1	4.34 ±1.3
All tasks (n=483)	5.38 ±3.1	4.01 ±2	4.17 ±2.1	4.00 ±1.9	3.78 ±1.8	3.33 ±1.8

Summed principal ground reaction force (∑PGRF) error results from the first k principal components (PCs), as well as all 45 PCs (i.e. original data). Eigenvalues λ_k represent the normalised amount of segmental acceleration variance explained by each PC_k. Root mean square errors (RMSE) are mean ± standard deviation values per PC_k for each task.

403

404

Appendix A: Principal segmental accelerations

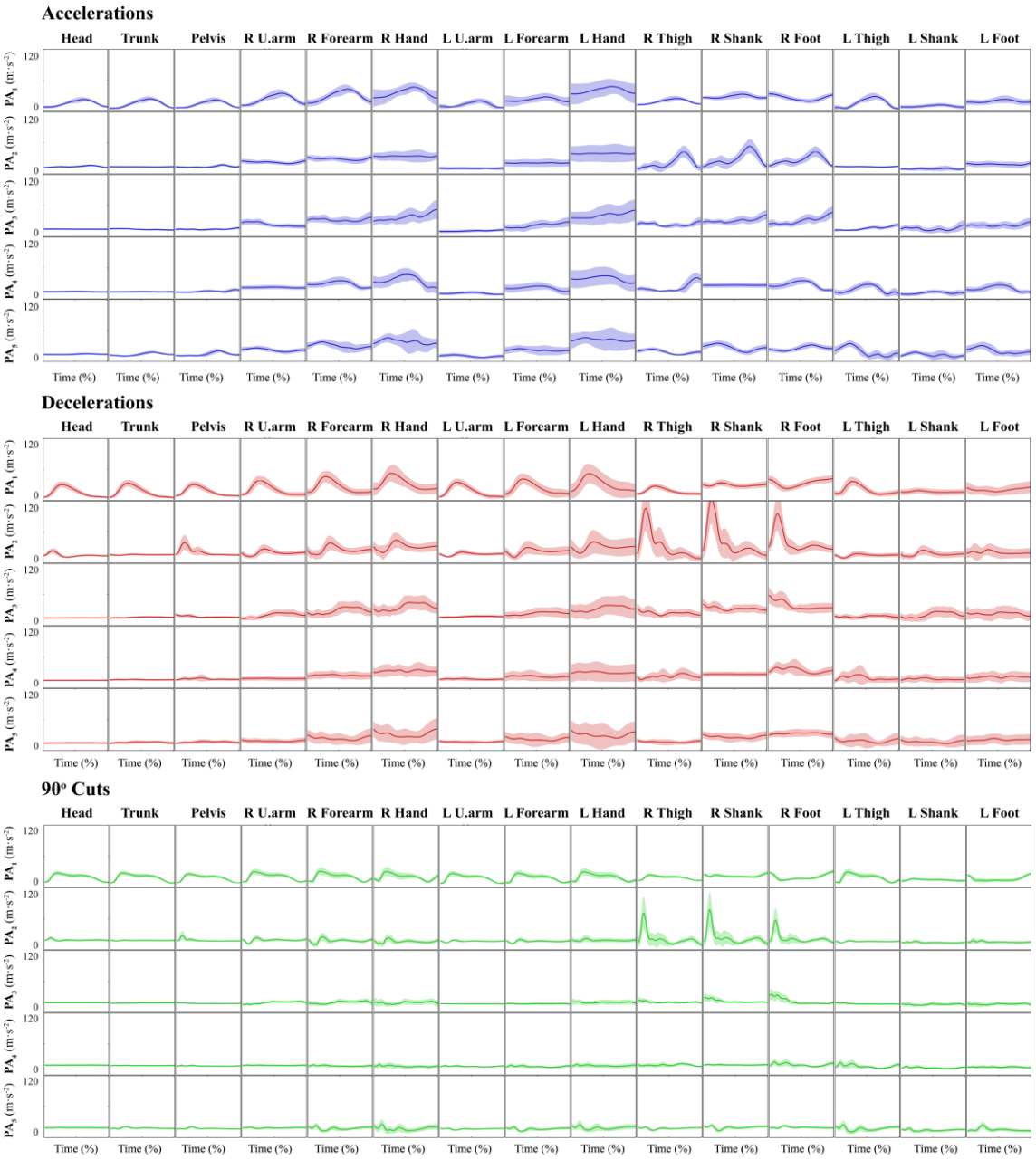

Figure A.1 Principal accelerations (PAs) from the first five principal components (rows) for accelerations (blue), decelerations (red) and 90° cuts (green) during a right leg contact phase. PA profiles are mean ± standard deviation (shaded) curves from 0-100% of stance, for all fifteen segments (columns).

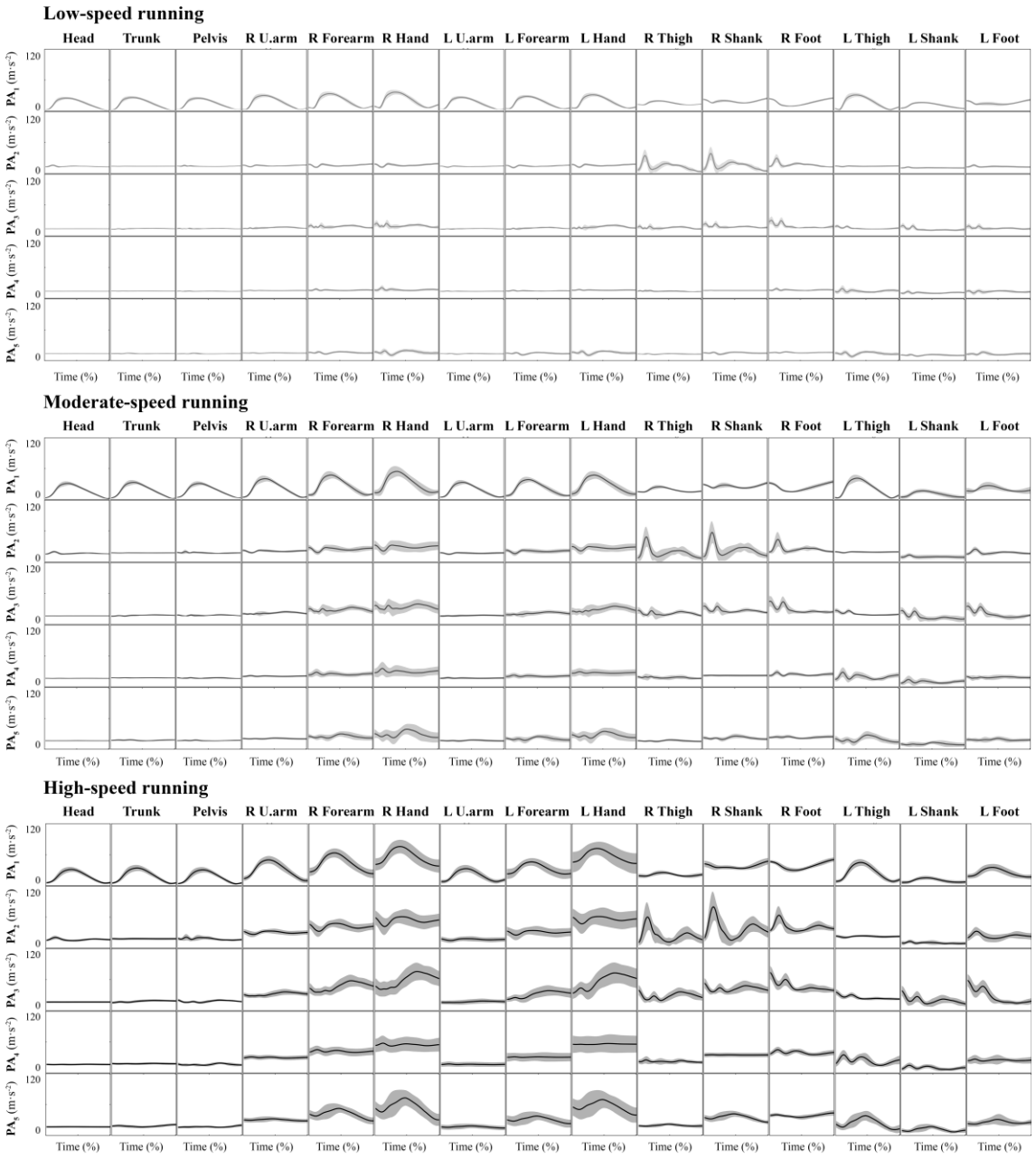

414 **Figure A.2** Principal accelerations (PAs) from the first five principal components (rows) for running
415 at constant low (light grey), moderate (grey) and high speeds (black) during a right leg contact phase.
416 PA profiles are mean ± standard deviation (shaded) curves from 0-100% of stance, for all fifteen
417 segments (columns).

418